Electrochimica Acta 357 (2020) 136861

Contents lists available at ScienceDirect

Electrochimica Acta

journal homepage: www.elsevier.com/locate/electacta

Corrosion behavior of AA2024-T6 and AA6065-T6 alloys in reline

Mihael Bucko[a], Alexandre C. Bastos[b], Kiryl A. Yasakau[b], Mario G.S. Ferreira[b], Jelena B. Bajat[c,*]

[a] University of Defense, Military Academy, 33 Pavla Jurisica Sturma St, 11000, Belgrade, Serbia
[b] CICECO – Aveiro Institute of Materials and DEMaC – Department of Materials and Ceramic Engineering, University of Aveiro, 3810-193, Aveiro, Portugal
[c] Faculty of Technology and Metallurgy, University of Belgrade, P.O. Box 3503, 11120, Belgrade, Serbia

ARTICLE INFO

Article history:
Received 28 January 2020
Revised 26 July 2020
Accepted 28 July 2020
Available online 5 August 2020

Keywords:
Deep eutectic solvent
Aluminum alloys
Corrosion
Reline

ABSTRACT

Deep eutectic solvents have been widely acknowledged as ionic liquid analogues, since they share many characteristics and properties with ionic liquids. The two major application areas of deep eutectic solvents have been metal processing and synthesis media; however, plenty of other applications have already been reported and predicted for these liquids. Reline, an eutectic mixture of choline chloride and urea, is a well known representative of deep eutectic solvents. Despite their importance in the contemporary technologies, the knowledge about the corrosivity of deep eutectic solvents is remarkably scarce. This article reports the results on the corrosivity of reline towards two Al alloys, namely AA2024-T6 and AA6065-T6. To measure the corrosion rates and characterize the passive film on the alloys in reline, electrochemical impedance and inductively coupled plasma optical emission spectroscopy methods were used, and the corrosion product composition was analyzed by X-ray photoelectron spectroscopy. Surface morphology and Volta potential were imaged by scanning electron microscopy, atomic force microscopy and scanning Kelvin probe force microscopy. The corrosion tests show that the two alloys are extremely stable in reline, and the passive layer is formed in the first three hours of immersion in the corrosive media. There is no evidence that electrolyte species are incorporated into the Al oxide protective layer through chemical bonding.

1. Introduction

The eutectic mixture of urea and choline chloride (commercial name reline) has been one of the most extensively investigated mixtures among the numerous deep eutectic solvents (DES) synthesized until now [1,2]. The properties of reline which favor its application in many fields, in comparison to water or organic solvents, include negligible vapor pressure, a wide electrochemical window, high thermal and chemical stability, high ionic conductivity, high solvating ability for some compounds insoluble in water, and inflammability – the properties generally attributed to ionic liquids [1,2]. The reline offers its potential application in areas like separation and absorption processes, organic synthesis, catalysis, electrochemistry, electroplating, heat transfer fluid, lubricant, etc. [1,2]. The important benefit of reline is the biodegradability of its constituent compounds: both urea and choline chloride are non toxic, renewable and biodegradable chemicals [3].

In order to apply reline in any large-scale process, it is important to gain knowledge about its corrosivity and interaction with different materials, particularly reactive metals and alloys. The research undertaken until now [4,5,6,7,8] has shown that the corrosion of Ni, Al, Cu, Ti, mild steel, and stainless steel in various choline chloride eutectic mixtures with urea, ethylene glycol and propylene glycol, is much lower compared to the corrosion of these metals in aqueous solutions.

The corrosion process of Al alloys in deep eutectic solvents has not been investigated until now. For this reason, in this work the corrosivity of reline towards two Al alloys, namely AA2024-T6 and AA6065-T6, has been investigated. The AA2024-T6 alloy possesses good combination of strength and fatigue resistance, due to the constituent particles, precipitates and dispersoids, based mainly on Cu with small amounts of Mg and Mn. Besides its applications in aerospace and automotive industry, it is used for various structural applications, gears for machinery, screw machine products, cylinders and pistons, fasteners, machine parts, packaging and rivets. The AA6065-T6 alloy is a general-purpose alloy, containing Mg-Si hardening precipitates, used for a broad range of structural applications and welded assemblies including pipelines, frames, agricultural applications, building products, chemical equipment, dump

* Corresponding Author
E-mail address: jela@tmf.bg.ac.rs (J.B. Bajat).

https://doi.org/10.1016/j.electacta.2020.136861
0013-4686/

bodies, electrical and electronic applications, fasteners, heat exchangers, evaporators, radiators, hospital and medical equipment, machine parts, and storage tanks [9,10]. The wide list of applications shows that it is expected that these alloys will be in contact with reline, as a new and promising electrolyte in many fields.

The corrosion resistance of Al in aqueous and non aqueous media depends on (a) the stability of the naturally formed Al_2O_3 layer, (b) the electrical conductivity of a medium, and (c) the presence of aggressive ions [11].

(a) For example, in aluminum electrolytic capacitors with organic electrolytes, the Al oxide withstands a potential range of 6–16 V [12]. It is also known [13] that anhydrous alcohols and phenols can severely corrode aluminium, but addition of up to 0.3 wt.% water usually stops corrosion by precipitating Al_2O_3.There are also examples of high corrosion resistance of Al alloys resulting from the protective action of a corrosion product other than Al_2O_3: Al dissolves rapidly in tetrahydrofuran (THF) + $A1C1_3$ + LiC1 electrolyte, but Al-Mg alloy shows excellent passivity, due to the low solubility of $MgCl_2$ as a corrosion product [14]. In relation to the described previous findings, low solubility values for Al_2O_3 in reline have been reported. In the two earlier works [3,15], metal oxides were added into choline chloride based DESs and the solubility was expressed as the measured metal content in DES. In the first study, in seven choline chloride based DESs after stirring for 2 h at 353–363 K, the solubility value for Al_2O_3 was between 0.1 and 0.2 wt.% - lower as compared to oxides of Ca, Ce, Cu, Zn, Pb, and Mo, but comparable to the values measured for Fe, Ce, and Pt oxides [3]. In the second study, the Al_2O_3 solubility in reline after 48 h at 333 K was even lower, < 1 ppm, and significantly lower than the solubility of Cu, Fe, Mn, Ni, Pb, and Zn oxides [15]. In another research, the Al_2O_3 was reported insoluble in the eutectic mixture of choline chloride, urea and ethylene glycol [16].

(b) The second parameter which could be used for the prediction of Al alloys corrosion in reline is its electrical conductivity. In a study of metal corrosion in various organic solvents (alcohols, acetone, diethyl ether, benzene, etc.) containing HCl, it was shown that the corrosion rate for Fe, Al, and Cr-Ni steel is very low in electrolytes with electrical conductivity lower than the threshold value of ~1 mS cm^{-1}, above which the corrosion rate increases rapidly [17]. For comparison, the reported conductivity of reline ranges from 0.24 to 6.36 mS cm^{-1} in the temperature range from 293.15 to 338.15 K [2]. Yet in media with aggressive adsorbed ions (like chloride in reline), the bulk conductivity of the medium does not allow for conclusions on the conditions at the metal/medium interface, because the surface conductivity might be high, in spite of the low bulk conductivity [18].

(c) The composition of the corrosive medium has a significant influence on the Al alloys´corrosion. As concerning the corrosivity of ionic liquids, the general rule for all metals is a significantly lower corrosion in neat ionic liquids as compared to water solutions, and even ionic liquids have been used as corrosion inhibitors for various metals in aqueous media [19]. The protective action of an ionic liquid is a result of an adsorbed multilayer of cations and anions of the ionic liquid, which isolate the metal surface from corrosive species in the electrolyte [19]. Yet it should be stressed out that some anions present in ionic liquids, may destroy the Al_2O_3 layer and induce Al corrosion: the examples are lithium salts like $Li[N(SO_2CF_3)_2]$ [20] and lithium imide [21].

Since reline contains ~5 mol dm^{-3} of chloride ion, it is extremely important to bear in mind that the susceptibility to localized corrosion for both AA2024 and AA6065 alloys, is higher than that for pure Al [22,23]. This is the result of the heterogeneity of the alloy surface, due to the existence of Al-Mg-Si precipitates at AA6065, and Al-Cu-Mg and Al-Cu-Mn-Fe precipitates at AA2024 alloy [22,23].

To summarize previous literature, the Al_2O_3 was reported as not completely insoluble at elevated temperature in reline, although the solubility is low, and the bulk electrical conductivity of reline could exceed the threshold value needed for rapid corrosion. Since it is important to have precise information regarding the behavior of Al alloys in this electrolyte during prolonged time of exposition, this work investigates in detail the corrosion of the two Al alloys in reline, by using electrochemical and non-electrochemical techniques.

2. Experimental

2.1. Materials and reagents

The AA2024-T6 and AA6065-T6 alloys were supplied by Mateck (Germany). Their chemical compositions, as given by the producers, are presented in Table 1. Reline was prepared from a 1:2 molar ratio mixture of choline chloride (ChCl) (Sigma-Aldrich, > 99%) and urea (Sigma-Aldrich, dry, >99.5%). The mixture was heated in a beaker at 80 °C and stirred until a homogeneous and colorless liquid was formed. Prior to mixing, both chemicals were dried overnight in oven at 60 °C and cooled to room temperature in a desiccator. After preparation reline was stored in bottles containing molecular sieves (L05335, 3A, Alfa Aesar) to absorb water, and the bottles kept in a desiccator.

2.2. Corrosion testing

In order to measure the corrosion rate of AA2024-T6 and AA6065-T6 in reline, the metallic samples were immersed in reline and held in the oven at 60°C. The corrosion testing was also performed in aqueous solution of 0.22 wt. % NaCl at room temperature, for comparison. The aqueous electrolyte composition was chosen in order to have the similar electrolytic conductivity as reline (~ 449 mS m^{-1}), so that the difference in the recorded results would not be a consequence of different conductivities.

The samples were electrically connected from the back and mounted in epoxy resin, so that only one side was in contact with the electrolyte. Before the immersion, the metal surface was abraded with emery papers of the following grades: 600, 1000, 1200, and cleaned in acetone. For all experiments involving immersion in the electrolyte, the samples were immersed immediately after the polishing.

Electrochemical impedance spectroscopy (EIS) was measured in reline or aqueous NaCl, in electrochemical cell with a three-electrode arrangement, consisting of the working electrode (resin mounted sample), a platinum counter electrode and saturated calomel electrode (SCE) as reference. The EIS measurements were performed at open circuit potential, with a 10 mV (rms) sinusoidal perturbation in the 100 kHz to 10 mHz frequency range and seven points per frequency decade. Electrochemical measurements were performed using a potentiostat ZRA Reference 600, Gamry Instruments. EIS 300 software was used for the fitting. The EIS testing was performed at two independent sets of samples, in order to ensure reproducibility.

Table 1
Chemical composition of AA2024-T6 and AA6065-T6 alloys, wt.%

	Cu	Mg	Mn	Fe	Si	Bi	Al
AA2024-T6	4.43	1.10	0.76	0.42	0.70	/	rest
AA6065-T6	0.33	0.95	0.05	0.20	0.55	0.65	rest

The metal content in reline due to corrosion was analyzed by inductively coupled plasma optical emission spectrometry (ICP-OES) using a Spectro Genesis spectrometer, with a Burgener nebulizer, a cyclonic spray chamber and radial viewing with 15 linearly positioned CCD detectors capable of measuring wavelengths from 175 to 777 nm.

2.3. Surface analysis by X-ray photoelectron spectroscopy (XPS)

Samples of AA2024-T6 and AA6065-T6 with surfaces polished to 1 μm alumina slurry were immersed in reline at 60 °C for 19 days. Then they were thoroughly washed with pure ethanol, dried, and stored in a desiccator for just a few hours before measurement. For comparison, similar samples were left in the laboratory ambient (23 ± 1 °C, 55 ± 5% RH) for the same 19 days and the surfaces also analyzed by XPS. The XPS analysis was performed on one sample for each case. The XPS spectra were acquired in Ultra High Vacuum (UHV), base pressure of 2×10^{-10} mbar, with a hemispherical electron energy analyzer (SPECS Phoibos 150), a delay-line detector and a monochromatic AlKα (1486.74 eV) X-ray source. High resolution spectra were recorded at normal emission take-off angle and with a pass-energy of 20 eV, which provides an overall instrumental peak broadening of 0.5 eV. No sputtering was performed to remove surface impurities. All spectra were corrected for adventitious C peak at 284.6 eV and the quantitative analysis was performed with the XPS PEAK 4.1 software.

2.4. Scanning Kelvin probe force microscopy (SKPFM)

Aluminum alloy samples about 1 × 1 cm were abraded with SiC paper down to 4000 grit and then polished by alumina pastes down to 0.1 micron. The samples were cleaned on a soft sponge pad wetted by 2-propanol and then dried on a filter paper. Samples were stored in a desiccator to prevent corrosion. Measurements were performed before and after 5 days of immersion in reline at 60 °C.

A Digital Instruments NanoScope III system with Extender^{TM} Electronic module was used to acquire topography and Volta potential difference (VPD) at the metallic surfaces. Atomic force microscopy (AFM) combined with SKPFM measurements were performed in a sequence. The first scan acquired topography of the surface. During the second scan the tip was lifted off from surface to a distance of 100 nm and using the nulling technique the VPD between the surface of the alloy and the tip was measured. Measurements were done at AC voltage amplitude of 5 V. Doped silicon probes covered with Pt-Cr layers, acquired from Budget sensors, were used for all AFM/SKPFM measurements. The VPD potential was carefully checked before and after measurements against a standard nickel metal surface [24]. Therefore, all VPD values are presented versus the Ni surface. Temperature and humidity during the measurements were around 23 ± 2°C and 52 ± 4% respectively. Scanning Electron Microscopy (SEM) pictures were acquired after immersion, in the same regions of SKPFM maps with a Hitachi S-4100 microscope. In order to achieve reproducible images, SKPFM, AFM and SEM imaging was performed at different surface places (at least three areas for each sample).

3. Results and discussion

3.1. Analysis of the surface composition

The reline contains organic cations and anions, chloride ions, water, and oxygen, while AA2024-T6 and AA6065-T6 alloys contain several chemical elements (Table 1). So, different surface films of Al alloys may be expected in reline. In order to identify potential products formed on the surface, AA2024-T6 and AA6065-T6 samples were exposed to air (as control samples) and immersed in reline at 60°C for 19 days, after which the XPS analysis of their surface was performed.

Fig. 1a shows the XPS overview spectra of the surfaces of all samples, while the high resolution XPS spectra of Al2p, O1s, N1s, Cl2p and C1s ionizations are presented in Figs. 1b – f, respectively. A first look at the spectra shows similar plots except for a few extra peaks in AA2024-T6 exposed to reline. The spectra of Al show two main peaks, one centered at 71.6 eV assigned to metallic Al (it is in fact two peaks for the ionizations of $Al2p_{3/2}$ and $Al2p_{1/2}$ with a spin orbit splitting of 0.44 eV) and a larger peak around 75 eV ascribed to the ionization of oxidized Al, with Al_2O_3 at 73.8 eV and $Al(OH)_3$ at 74.6 eV. The deconvolution of the O1s spectra gives two peaks, one for O^{2-} at 530.7 eV and another due to OH^- at 531.8 eV. Nitrogen showed a small peak around 399.7 eV in all surfaces, probably related to some sort of contamination. A stronger peak manifested in the AA2024-T6 sample immersed in reline with binding energy of 402.5 eV, which is attributed to the ionization of N1s from a quaternary amine such as choline cation. If choline is on the surface, then the counter anion chloride should also be present. Indeed, peak of Cl^- ionization at 197.5 eV appears in the same sample. The peak is divided in two, reflecting the ionization of $Cl2p_{3/2}$ and $Cl2p_{1/2}$ with a spin orbit coupling of 1.22 eV. Carbon presented two main peaks plus a third one of lower intensity. The first, at 284.6 eV, is attributed to adventitious carbon, the second, around 286 eV, is related to C-O, and the third at 288 eV is assigned to C=O. This carbon comes from the surface contamination. The stronger C-O peak in AA2024-T6 immersed in reline is explained by the present of the C–OH of choline cation.

It is concluded that the XPS peaks are similar for all samples except for the existence of some choline chloride deposits on the surface of AA2024-T6 exposed to reline, that were not washed with ethanol. The XPS results suggest that the oxide films developed in reline with the inherent small amount of water and dissolved oxygen are not different from the ones formed in atmospheric mild conditions (23 ± 1 °C, 55 ± 5% RH).

The XPS peak deconvolution process is presented in the supplementary material, and the deconvolution results are given in Tables 2 and 3.

In conjunction with XPS analysis, the visual appearance of the samples immersed in reline at 60 °C, as well as those kept in the laboratory environment for 19 days, is presented in Fig. 2. The surfaces of all samples were still shiny after 19 days of exposure. No corrosion or just benign signs of corrosion could be observed. The surfaces immersed in reline (Fig. 2b,d) seem to have some brownish deposits as compared to the samples exposed to air, however the closer look by scanning electron microscope (Fig. 2f) showed that there was no corrosion product deposits, and that spots seen on AA2024-T6 after 19d in reline were not pits but rather only electrolyte deposits not removed by the washing process with ethanol. So, there were no detected points of attack, i.e., neither pitting or clear proofs of localized corrosion. On the other hand, in some samples gas bubbles appeared in the first hours of immersion, probably due to hydrogen evolution in localized points, but they did not further increase in size or number until the end of the test (Fig. 2e). It was the initial corrosion, probably originating by the small amount of water that existed in the electrolyte. This corrosion did not last long, i.e. either the surface became more passive with time or the water was consumed.

3.2. Electrochemical measurements

The open circuit potential, E_{ocp}, of the two alloys immersed in two different electrolytes was monitored for 33 days (Fig. 3). In aqueous 0.22 wt. % NaCl solution, the E_{ocp} of both samples dif-

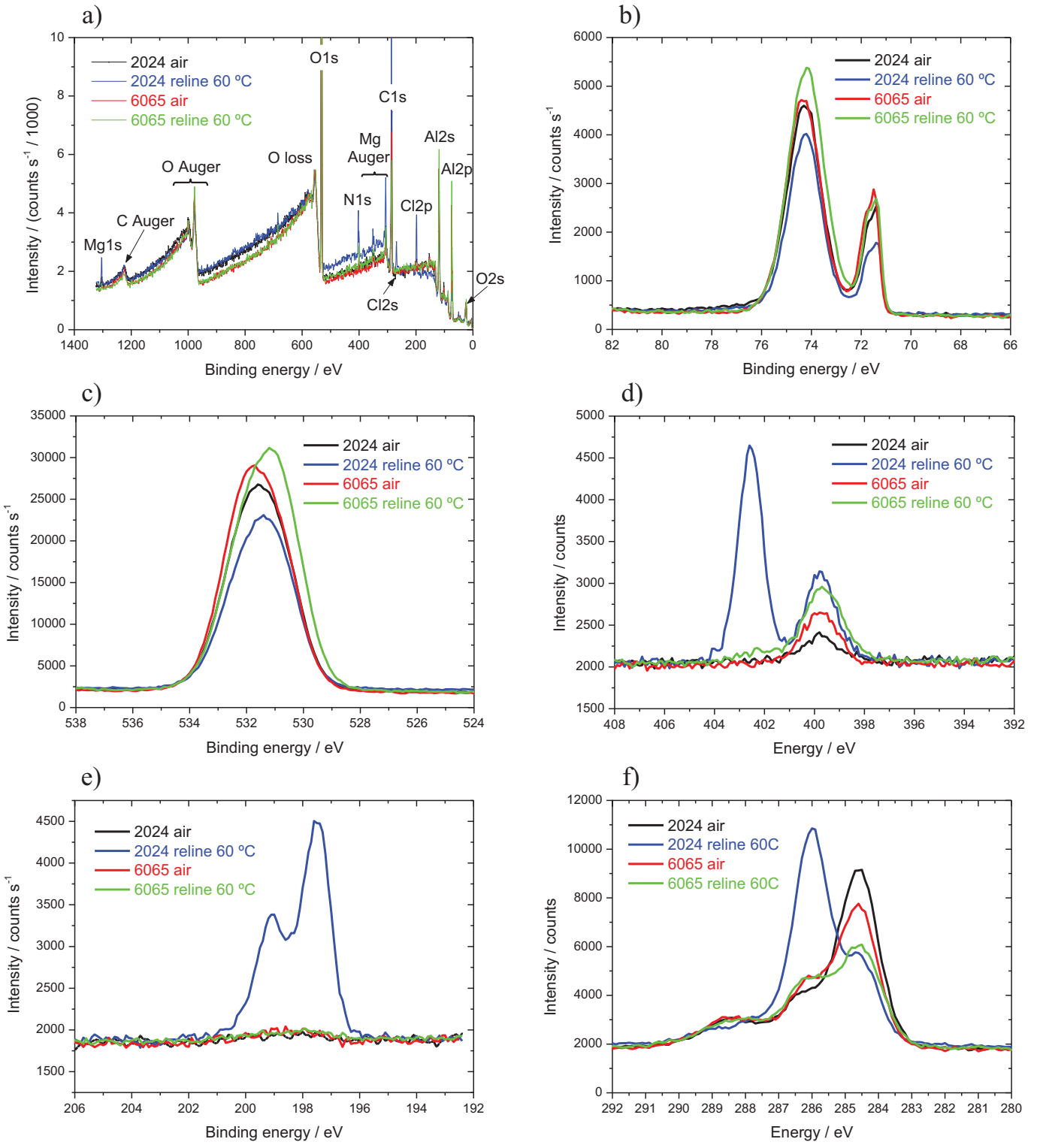

Fig. 1. XPS analysis of AA2024-T6 and AA6065-T6 after 19 days in laboratory environment (23 ± 1 °C, 55 ± 5% RH) and immersed in reline at 60 °C. a) overview spectra, and high resolution spectra of b) Al2p, c) O1s, d) N1s, e) Cl2p, and f) C1s.

fers a little and shifts toward negative values with immersion time. The initial E_{ocp} values of both samples in reline are more negative than in NaCl, but they sharply increase with time during the first week of exposure to reline. This is followed by E_{ocp} stability. The E_{ocp} oscillations at the early immersion in reline (inset in Fig. 3) are the result of changes on the electrode, like layer formation, which eventually leads to potential ennoblement in reline. It can be also seen from Fig. 3 that the initial potential difference, of about 200 mV, among the samples, was significantly reduced after about 12 days.

The EIS measurements were further performed on AA2024-T6 and AA6065-T6 samples immersed in reline for 37 days and the results were compared with those recorded in 0.22 wt.% NaCl aqueous solution. The comparative impedance data measured at open

Table 2
Quantification of the XPS spectra of AA2024-T6

		Air			reline		
		B.E. (eV)	FWHM (eV)	%	B.E. (eV)	FWHM (eV)	%
Al2p	Al^0	71.6	0.9	5.0	71.6	0.9	4.0
	Al_2O_3	73.9	1.4	11.9	73.8	1.1	7.8
	$Al(OH)_3$	74.6	1.2	10.2	74.6	1.3	12.7
O1s	O^{2-}	530.6	1.7	10.1	530.6	1.6	9.6
	OH^-	531.8	2.2	32.9	531.8	2.2	24.3
C1s	C-C/C-H	284.6	1.4	19.5	284.6	1.4	6.9
	C-O	286.2	1.3	4.5	286.0	1.2	16.1
	C=O (?)	288.2	2.3	4.9	287.7	2.4	9.2
Mg1s	Mg^0	1304.1	1.8	0.4	1304	2.0	0.5
N1s	NH_2 (?)	399.8	1.6	0.6	399.7	1.5	1.6
	NR_4^+	-	-	-	402.6	1.1	3.3
Cl2p	Cl^-	-	-	-	197.5	1.2	3.8

Table 3
Quantification of the XPS spectra of AA6065-T6

		air			reline		
		B.E. (eV)	FWHM (eV)	%	B.E. (eV)	FWHM (eV)	%
Al2p	Al^0	71.6	0.9	5.5	71.6	0.928	4.9
	Al_2O_3	73.8	1.2	8.4	73.9	1.55	14.3
	$Al(OH)_3$	74.6	1.3	13.1	74.6	1.42	10.2
O1s	O^{2-}	530.7	1.7	9.8	530.6	1.87	16.4
	OH^-	532.0	2.1	25.9	531.9	2.2	21.5
C1s	C-C/C-H	284.6	1.4	20.6	284.6	1.58	17.1
	C-O	286.1	1.4	8.9	286.2	1.29	7.4
	C=O (?)	288.3	2.2	6.9	288.1	2.56	6.6
Mg1s	Mg^0	1304.2	1.9	0.05	1303.9	1.99	0.06
N1s	NH_2 (?)	399.8	1.6	0.85	399.6	1.88	1.5

circuit potential are shown in Figs. 4 and 5. After 3 h of immersion, the Nyquist plot is shaped into one semicircle (Figs. 4a and b), indicating one time constant or, possibly two not well separated time constants. This response does not change during the total immersion time, for both alloys. The impedance increased monotonically with the immersion time, and at the end of experiment, the impedance response resembled capacitive behavior. An almost vertical line parallel to the axis of the ordinate, characterizes the electrolyte/Al interface separated by a dielectric, Al_2O_3 [12,25].

The impedance values in reline were two orders of magnitude higher than the ones recorded in NaCl solution (Figs. 4c and 5 a and b). Besides, the shape of spectra, with resistive semicircles and well resolved time constants in NaCl, suggest that a fast electrochemical process occurs at both samples in NaCl, unlike more capacitive response observed for samples immersed in reline. Therefore, the corrosion process in reline is significantly lower comparing to the water solution, in spite of a much higher Cl^- ion concentration (~5 mol dm^{-3} in reline *vs.* 3.75 • 10^{-2} mol dm^{-3} in aqueous solution). These results correlate well with the evolution of open circuit potential with immersion time, where it was shown that the E_{ocp} ennoblement in reline suggests the formation of passive film.

The fitting procedure by EIS 300 Gamry software has shown that the best agreement with the measured data in reline was achieved when the equivalent electrical circuit (EEC) included two time constants. It is known that the process when electrolyte penetrates into the pores of Al_2O_3 layer could be characterized with the two time constants in the EIS diagram [12]. The simple equivalent circuit for fitting such system is offered in earlier literature [12,25,26] and is given in Fig. 6. Besides the solution resistance (*Rs*), the time constant at higher frequencies is the response of the passive oxide film (C_{ox}/R_{ox}) and the other one, at lower frequencies, corresponds to the response of areas not covered by the passive layer, where the alloy is directly in contact with the solution. In these pores, the metal dissolution is controlled by the charge transfer resistance, R_{ct}, and the electrochemical double layer is characterized by capacitance C_{dl}. In fitting procedure, constant phase elements *CPE* were used instead of pure capacitors, since the capacitance response was not ideal. The capacitance of the system was calculated using EIS 300 software, from the fitted results for CPE, according to the Eq. 1:

$$C = \frac{(Y * R)^{1/n}}{R} \quad (1)$$

where *C* represents the real capacitance, while *Y* and *n* represent the fitted values of capacitance and exponent for CPE element, respectively.

The Fig. 7 presents the fitted resistance and capacitance values obtained for different immersion times in reline, determined by modeling with the EEC in Fig. 6. The goodness of fit using nonlinear least squares fitting algorithm was $< 10^{-3}$. According to the resistance values, the oxide layer becomes more compact and resistant over time. The resistance of the oxide itself increases monotonically over the entire immersion period (Fig. 7a). Contrary, the charge transfer resistance in the oxide pores, increases dramatically during the first three days (from ~10^6 to ~10^7 Ω cm^2). After this period, equivalent fitting of the EIS spectra may be accomplished by using a single time constant equivalent electrical circuit, which is related to a homogeneous oxide layer. This means that the majority of the pores in the protective film, where the metal dissolution may proceed, gradually close and become smaller in number and size within the first three days. The values of the capacitance of the oxide film, calculated from the fitting data for *CPE* element, are in a very narrow range (1.5–3.2 μF cm^{-2}) during the whole immersion experiment for both alloys (Fig. 7b). The order of the magnitude of μF cm^{-2} denotes that this is the capacitance of the oxide passive layer [11].

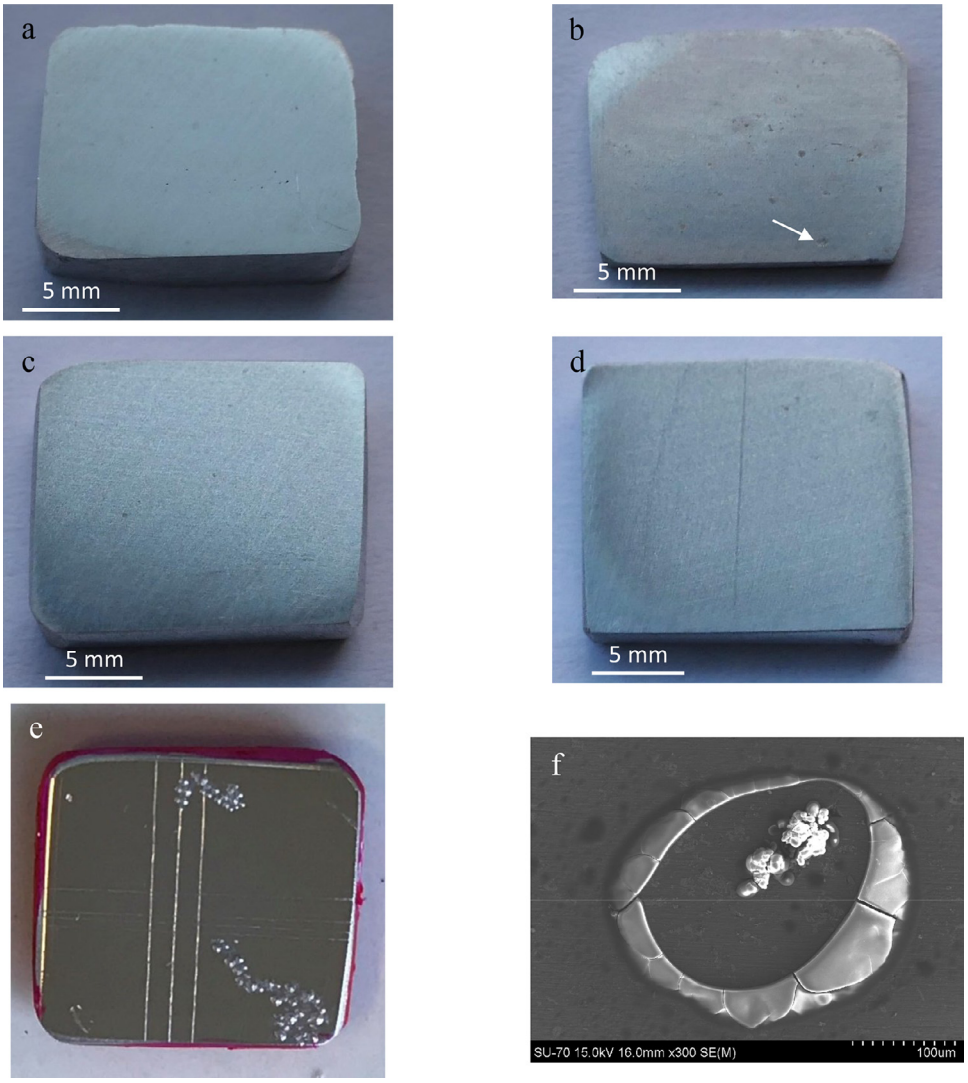

Fig. 2. Visual inspection of the alloy samples after 19 days: a, c) AA2024-T6, AA6065-T6 in the lab environment; b, d) AA2024-T6, AA6065-T6 in reline, respectively, e) AA2024-T6, a few hours after the immersion in reline, and f) detail of the point marked with an arrow in b).

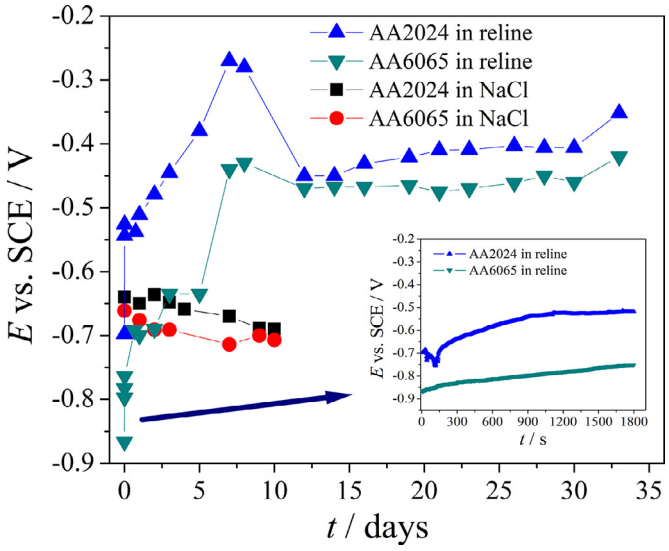

Fig. 3. E_{ocp} in 0.22 wt. % NaCl and reline for long immersion, inset: in reline for short immersion

The capacitance information in Fig. 7b was used to calculate the Al_2O_3 layer thickness using the procedure described in [11]: total capacitance values obtained in the fitting procedure are assumed to be partly due to the oxide layer, and partly due to the Helmholtz layer. The oxide and Helmholtz layers are treated as serialized capacitors, where the equivalent capacitance is expressed in Eq. 2:

$$C_{ox}{}^{-1} = C_H{}^{-1} + C_\delta{}^{-1} \quad (2)$$

Where C_{ox}, C_H, C_δ are the total capacitance, Helmholtz layer capacitance (the assumed value was 50 μF cm^{-2} [11]), and oxide film capacitance, respectively. The C_δ values calculated in this manner were then used to calculate the Al_2O_3 layer thickness, according to the Eq. 3:

$$\delta = \varepsilon\, \varepsilon_0 C_\delta{}^{-1} \quad (3)$$

where δ, ε, and ε_0 are the oxide thickness, the relative dielectric constant for oxide layer, and the permittivity of free space, respectively. A range of values between 9 and 40 was suggested in the literature for the relative dielectric constant, and the exact value depends on the degree of hydration of the passive layer: the less hydrated oxide has lower dielectric constant [11,26].

The calculated δ values are plotted in Fig. 7c for different immersion times and two different assumed ε values. In analogy to

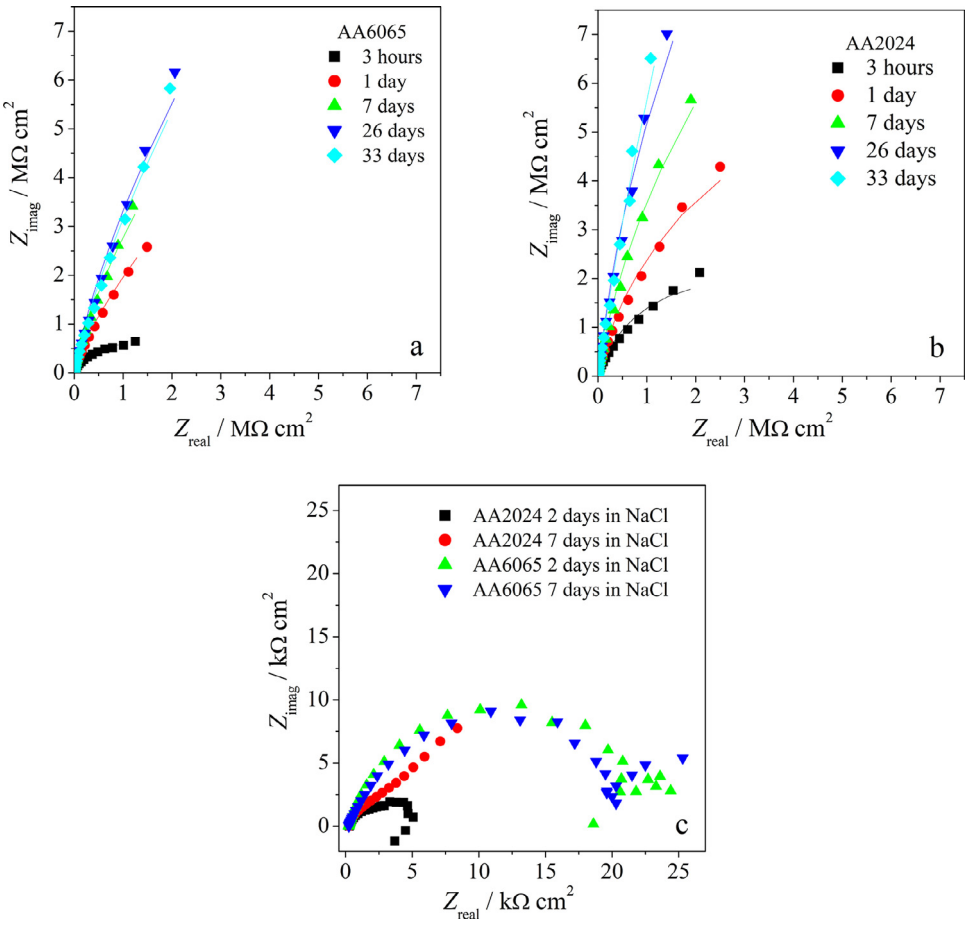

Fig. 4. EIS measurements of: a) AA6065-T6 in reline, b) AA2024-T6 in reline and c) AA6065-T6 and AA2024-T6 in 0.22 wt. % NaCl. Symbols are experimental data and lines are the fit results.

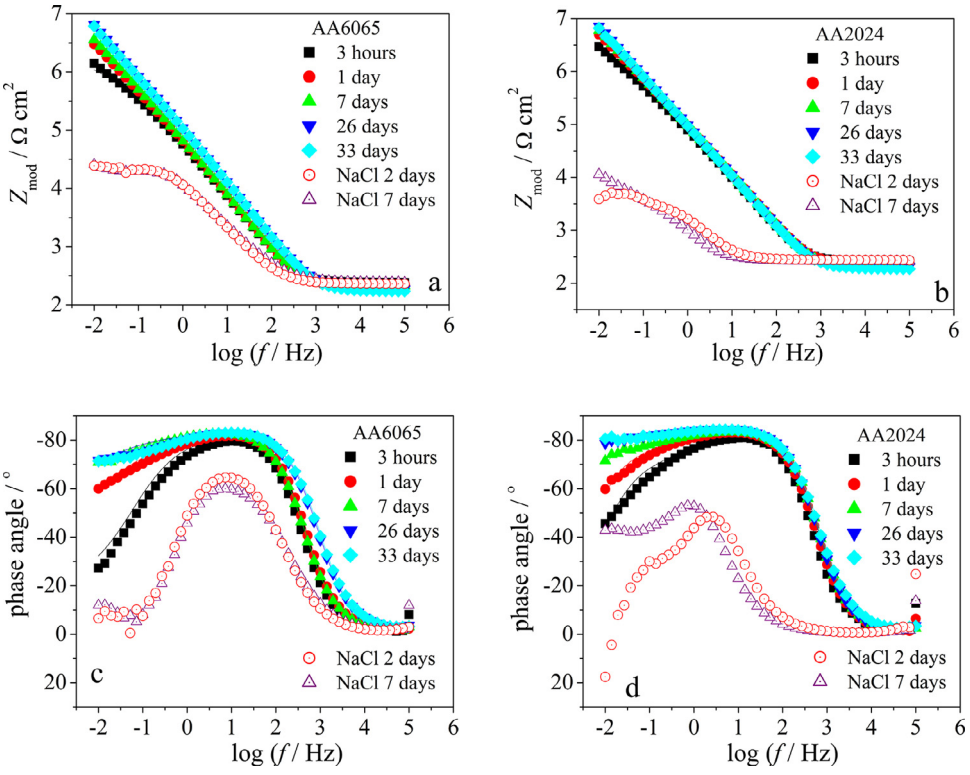

Fig. 5. Bode modulus (a and b) and phase angle (c and d) plots of AA6065-T6 (a, c) and AA2024-T6 (b, d) in reline and 0.22 wt. % NaCl. Symbols are experimental data and lines are the fit results.

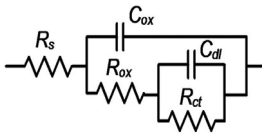

Fig. 6. Equivalent electrical circuit for metal/oxide/electrolyte interface.

the capacitance values, the oxide film thicknesses do not oscillate much over time, and no difference is observed for the different alloy samples. The calculated values are very similar to the Al_2O_3 layer thickness reported previously: in [26] the thickness of Al_2O_3 formed in aqueous solutions at different Al alloys and Al single crystals, was between 1.6 and 7 nm; in [11] the thickness of 4–5 nm was measured at potentiostatically polarized Al in aqueous NaCl. This correlation with previously investigated systems gives evidence that the EIS data in this work, describe the behavior of Al_2O_3 layer on the two alloys. It is interesting to note that the steady oxide thickness is formed already in the first day of immersion, and this value is maintained through the immersion experiment.

Summarizing EIS data show that the AA2024-T6 and AA6065-T6 alloys are very resistant in reline, over prolonged time of immersion: the protective oxide film is formed quickly and its compactness increases with time. The class of organic electrolytes non corrosive to Al and its alloys is broad, and reline obviously belongs to this class as well. Some representatives of such electrolytes are organic solvents with dissolved $LiPF_6$, $LiBF_4$, LiF, etc., used in lithium ion batteries [27], or solvents used in Al electrolytic capacitors, like ethylene glycol and γ-butyrolactone [12].

3.3. Surface morphology

The surface changes after immersion in reline were investigated by atomic force microscopy, scanning Kelvin probe force microscopy and scanning electron microscopy, with measurements made before and after 5 days in reline at 60 °C. The results of AA2024-T6 and AA6065-T6 are presented in Figs. 8 and 9, respectively. The samples were polished prior to testing and the surfaces remained smooth after immersion, as confirmed by the topography maps and the profile lines – Figs. 8 and 9, a), c) and e).

The VPD between intermetallics and alloy matrix containing second phase is directly related to the distribution of these elements in the alloy, which, in turn, depends on the heat treatment and aging. Before immersion, the intermetallic particles (IMPs) in AA2024-T6 are S-phase (Al_2CuMg) and FeMn-rich phases shown in Fig. 8 g and h, as well as Cu and Mg containing second phase particles that could not be seen in SEM images [28]. And in AA6065-T6, the existing IMPs are Si-rich phases [29], seen in Fig. 9 g,h, as well as Mg and Si containing hardening precipitates that could not be detected by SEM. The observed IMPS presented VPD with values up to 200 mV more positive than the surrounding aluminum matrix. The VPD for the aluminum matrix was around -0.725 V vs Ni for AA2024-T6 and about -1.0 V vs Ni for AA6065-T6. After 5 days in reline the measured VPD shifted to more positive values, close to -0.550 V vs Ni for AA2024-T6 and between -0.600 and -0.650 V vs Ni for AA6065-T6. The potential differences between IMPs and aluminum matrices were substantially decreased after exposure to reline.

After immersion, the samples were inspected by SEM in the exact places of the Volta potential measurements – Figs. 8 and 9, g) and h). The surfaces were undamaged, with the IMPs easily observed and no signs of localized attack neither on the alloy matrix nor around the intermetallics.

The loss of VPD contrast between IMPs and aluminum matrix upon immersion in reline, the general potential shift to more positive values and the absence of corrosion, namely around the IMPs, suggest the formation of a protective passive layer. These results are in good correlation with EIS results.

The microstructure of both alloy samples after 3 days immersion in 0.22 wt. % NaCl solution (Fig. 10) show visible signs of pitting, in the form of trenching around IMPs, in clear contrast to the

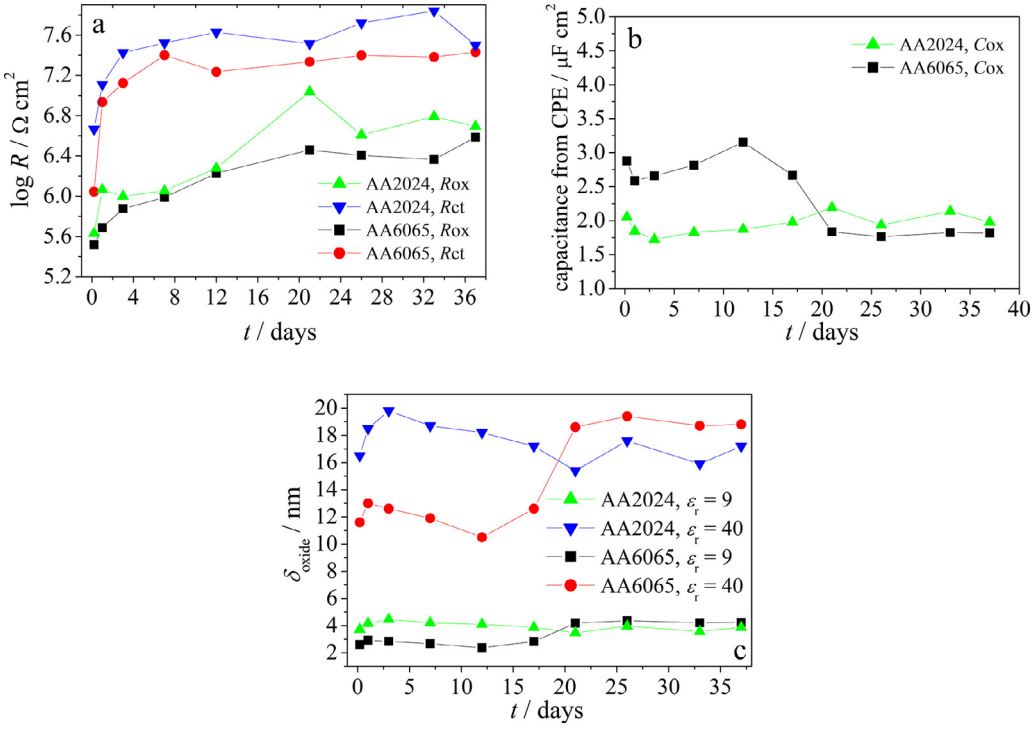

Fig. 7. a) Resistances (R_{ox} and R_{ct}), b) oxide capacitance, and c) oxide thickness values obtained from fitting the circuit in Fig. 6 to the recorded EIS data.

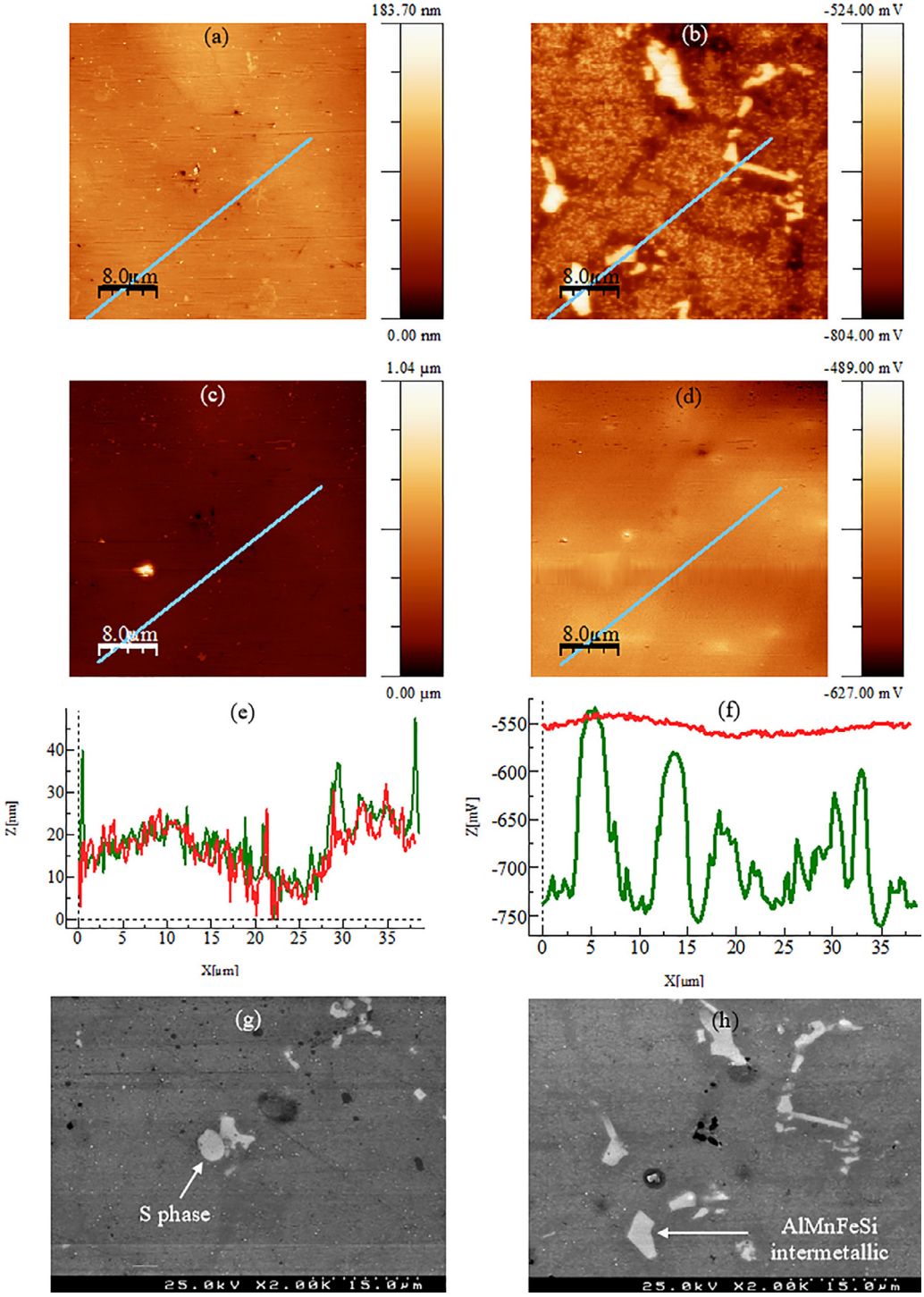

Fig. 8. AFM, SKPFM and SEM of AA2024-T6. a) and c) topography maps, b) and d) Volta potential maps, a) and b) before immersion, c) and d) after 5d immersion in reline at 60 °C; e) height profile in lines indicated in the maps, f) Volta potential profile in the lines indicated in the maps (green line: before, red line: after immersion), g-h) SEM images of AA2024-T6 surface after 5d in reline at 60 °C (h corresponds to area of maps b-d). Volta potential differences are presented versus Ni reference metal.

observations in reline. So, corrosion of both alloy surfaces was localized, on intermetallic particles and around precipitates, what is typical in chloride containing aqueous media.

3.4. ICP-OES measurements

The ICP-OES technique estimates the amount of metal ions released to the corrosive medium from the metal surface over time. It may not be used for precise measurement of the corrosion rate. For example, in case of Mg corrosion, it is known that ICP method gives corrosion rate ~40% lower as compared to the rate measured from mass loss test [30]. Yet this method gives the corrosion rates of the same order of magnitude as other methods, and it could be useful in this work for comparison with the electrochemical impedance spectroscopy results.

The concentration of Al^{3+} ion in reline and NaCl solution over time is presented in Fig. 11a. The results are obtained as average values from three independent measurements. Interestingly, al-

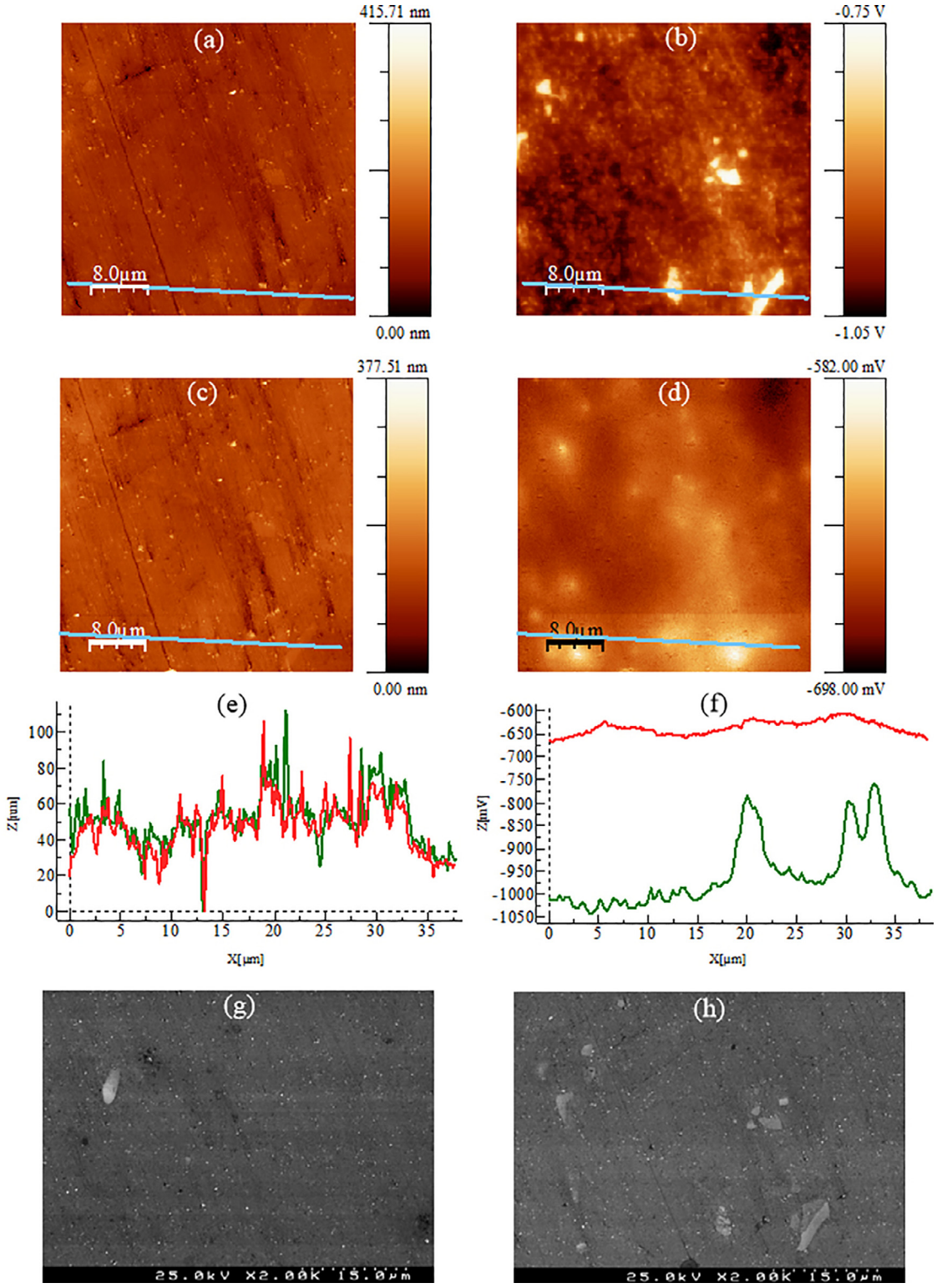

Fig. 9. AFM, SKPFM and SEM of AA6065-T6. a) and c) topography map, b) and d) Volta potential map, a) and b) before immersion, c) and d) after 5d immersion in reline at 60 °C; e) height profile in lines indicated in the maps, f) Volta potential profile in the lines indicated in the maps (green line: before, red line: after immersion), g-h) SEM images of AA6065-T6 surface after 5d in reline at 60 °C (h corresponds to area of maps b-d). Volta potential differences are presented versus Ni reference metal.

though AA2024-T6 and AA6065-T6 contain Cu, Mg, Zn, Mn and Si as alloying elements, the released amount of these metals in reline is below the detection limit of ICP OES. In NaCl solution, the ICP has detected Mg and Mn ions besides Al, which is understandable considering their negative potentials. As expected, the Al^{3+} ion shows the highest concentration in reline among all alloying elements, however its concentration changes over time with the same pattern for both alloys. It is seen that the concentration increases in the first 100 h for AA6065-T6, and 200 h for AA2024-T6, and then continually decreases. This behavior suggests the formation and growth of a passive layer during immersion time and once the critical thickness of the oxide layer is formed the metal

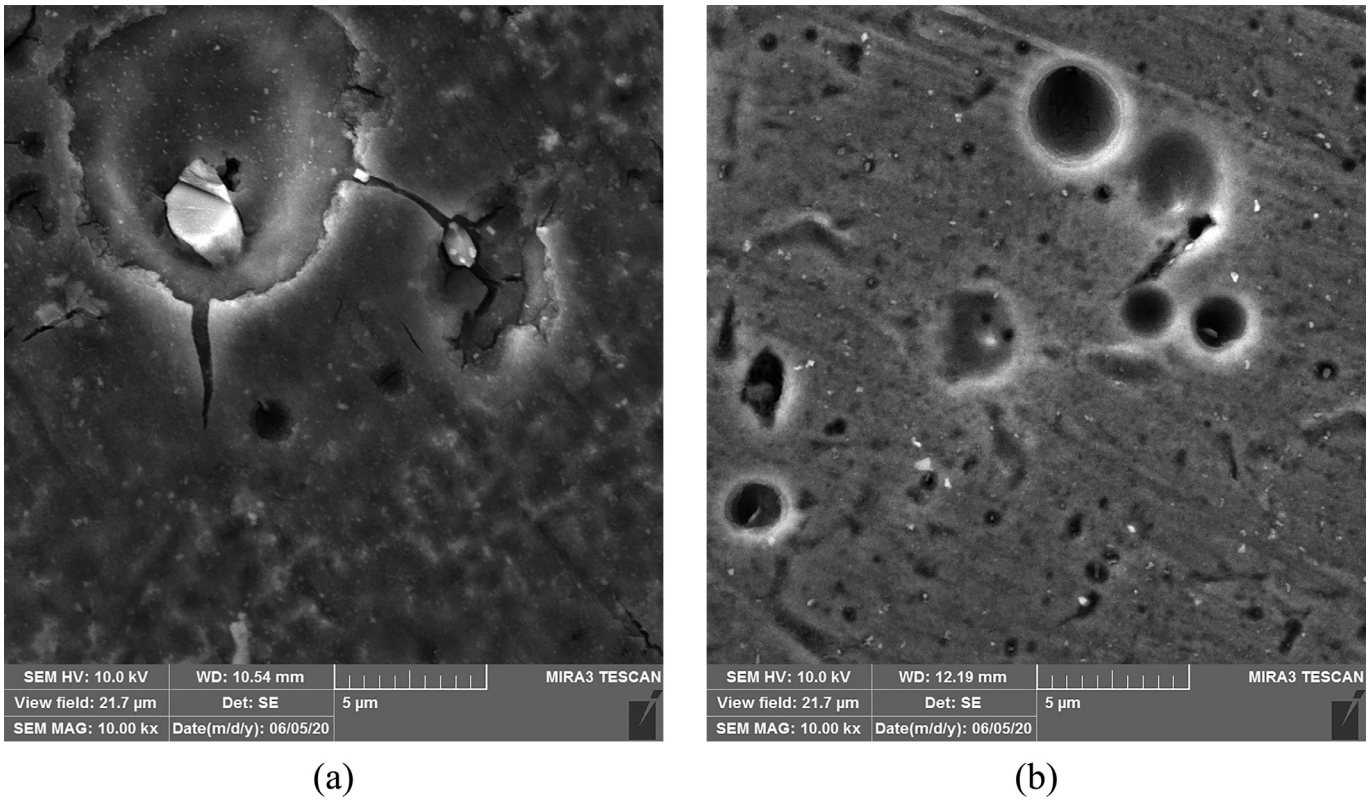

Fig. 10. SEM images of a) AA2024-T6 and b) AA6065-T6 after 3 days immersion in 0.22 wt. % NaCl.

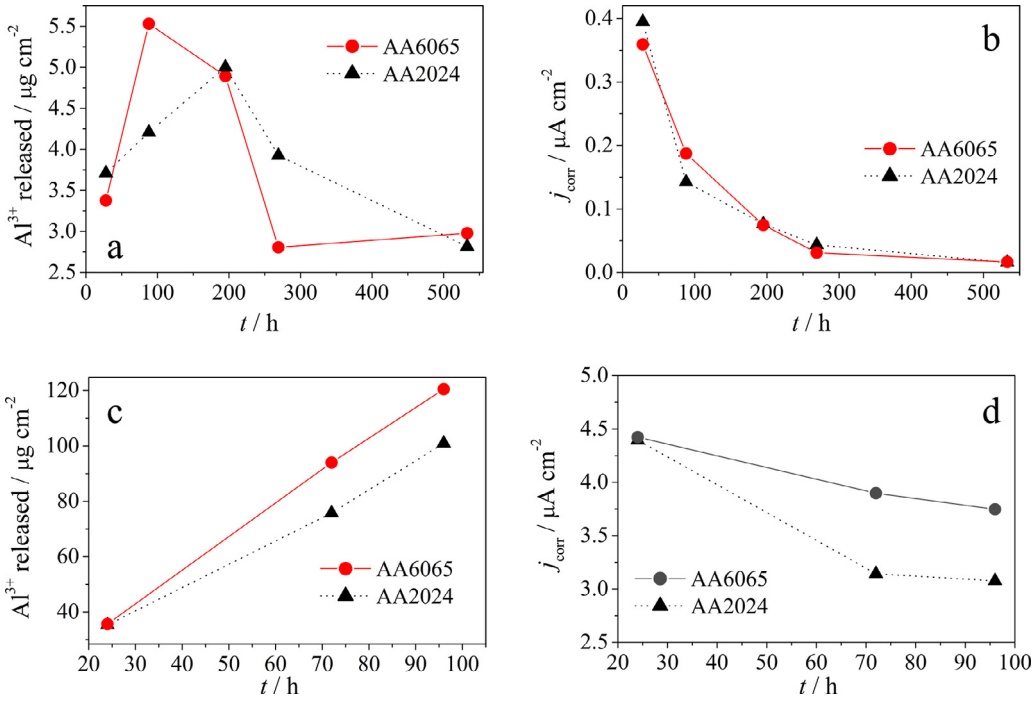

Fig. 11. Metal concentration measured by ICP-OES over time (a, c) and the corresponding calculated corrosion current density (b, d), in reline (a, b) and in 0.22 wt. % NaCl solution (c, d).

release into the electrolyte becomes lower. The ICP measurements of ions released to 0.22 wt. % NaCl solution (Fig. 11c) show that the metal concentration at the beginning of immersion is around ten times higher as compared to the case of reline, and it continually increases, indicating that a continual active dissolution occurs in this medium.

The amount of Al released to reline was used to calculate the corrosion current density using the Faraday law, and the results are given in Fig. 11b. Even at the beginning of immersion, the calculated corrosion current density is low ($< 0.5\ \mu A\ cm^{-2}$) and an order of magnitude lower than in NaCl (Fig. 11 d). After ~150 h, it

decreased below 0.1 μA cm^{-2}, which means a negligible corrosion rate.

3.5. Protection role of organic compounds in reline

One may suggest that the observed high corrosion resistance of Al alloys in reline may be a consequence of several different processes: protection of the metal surface by adsorbed organic molecules; insufficiency of Cl^- ions to cause pitting; or mass transport limitation of the corrosion process.

a) It is well known that Cl^- ion causes instability of the passive film and leads to its breakdown. However, it was also proven that some minimal surface coverage by Cl^- ion is necessary to induce the rupture of the oxide film, and below this threshold, chloride ions have little effect [31,32]. Accordingly, the simplest justification of a high resistance of Al_2O_3 film in reline could be the insufficient coverage of the film by Cl^-, as a consequence of the specific structure of a metal/reline interface. Various structures of the electrochemical double layer in reline have been reported, depending on the substrate. The surface of Hg in choline chloride based DESs [33] is covered with a layer of HBD molecules in the whole potential range. On the other hand, the interfacial layer at Pt in contact with reline is enriched with choline cations at negative potential relative to OCP and at OCP, while chloride anions at positive applied potentials [34]. Therefore, the two examples for Hg and Pt in reline, support the possibility that either urea molecules or choline cations constitute the first liquid layer in contact with the Al_2O_3 surface, so the solid surface is separated and protected from Cl^- anions.
b) In addition to the suggested role of adsorbed molecules, the slow dissolution of passive layer may be simply ascribed to the limited availability of suitable ligands in the deep eutectic solvent that may complex Al ions. It must be held in mind that although the reline contains high concentration of Cl^- ion, the complexation of this ion with urea molecules ensures that the Cl^- activity is effectively very close to zero. Hence the dissolved Al^{z+} species must compete with urea molecules for the halide ligand [35].
c) Finally, the high reline viscosity and low diffusivity of species in this liquid, ensure that the pitting corrosion, even if it occurs at some point, will be terminated due to the mass transport limitation. Earlier work has shown that the formation of a stable pit is controlled by diffusion of metal cations within the pit [36]. This was confirmed in many organic solutions [36], but also in highly concentrated, highly viscous aqueous chloride solutions [37].

4. Conclusions

The deep eutectic mixture of choline chloride and urea is recognized as a promising electrolyte and solvent in various applications, and so the corrosivity of this mixture towards metals is one of its important characteristics. The electrochemical and ICP OES measurements have shown that the corrosion rates of AA2024-T6 and AA6065-T6 alloys in reline are extremely low, classifying reline into the group of non corrosive media. The electrochemical impedance studies denote that the passive film is formed on the Al alloys already after three hours of immersion in reline at 60 °C, and the compactness and thickness of the film steadily increase over time. A two time constant equivalent circuit was used for modeling the EIS data, where one time constant represented the oxide film, and the second time constant was related to the electrochemical process on the exposed metal due to the ingress of the electrolyte into the oxide film pores.

The analysis of the surface film composition by XPS technique has shown that the film produced on Al alloys immersed in reline, is aluminum oxide/hydroxide, with no evidence of any chemical bonds with choline cation, urea molecule or chloride anion. Therefore, the passive behavior of Al alloys in reline was ascribed to the very low solubility of Al oxide in reline.

Declaration of Competing Interest

The authors declare that they have no known competing financial interests or personal relationships that could have appeared to influence the work reported in this paper.

CRediT authorship contribution statement

Mihael Bucko: Conceptualization, Investigation, Writing - original draft. **Alexandre C. Bastos:** Conceptualization, Investigation, Writing - original draft. **Kiryl A. Yasakau:** Investigation. **Mario G.S. Ferreira:** Resources, Validation. **Jelena B. Bajat:** Conceptualization, Methodology, Resources, Supervision.

Acknowledgements

This research was financed by the Ministry of Education, Science and Technological Development of the Republic of Serbia (Contract No. 451-03-68/2020-14/200135). The authors would like to acknowledge support for Serbia-Portugal bilateral project (337-00-00227/2019-09/80). ACB acknowledges FCT—Fundação para a Ciência e a Tecnologia, I.P., in the scope of the framework contract foreseen in the numbers 4, 5, and 6 of the article 23, of the Decree-Law 57/2016, of August 29, changed by Law 57/2017, of July 19. K.A. Yasakau thanks the Portuguese Foundation for Science and Technology (FCT) and "Programa Operacional Capital Humano, comparticipado pelo Fundo Social Europeu e por fundos nacionais do MCTES" for the financial support and Researcher grant (IF/01284/2015). Project CICECO – Aveiro Institute of Materials – UIBD/CTM/50011/2020 and UIBP/CTM/50011/2020, financed by national funds through the FCT/MCTES, and when appropriate co-financed by FEDER under the PT2020 Partnership Agreement is also acknowledged.

Supplementary materials

Supplementary material associated with this article can be found, in the online version, at doi:10.1016/j.electacta.2020.136861.

References

[1] E. Smith, A.P. Abbott, K.S. Ryder, Deep eutectic solvents (DESs) and their applications, Chem. Rev. 114 (2014) 11060–11082, doi:10.1021/cr300162p.
[2] V. Agieienko, R. Buchner, viscosities Densities, and electrical conductivities of pure anhydrous reline and its mixtures with water in the temperature range (293.15 to 338.15) K, J. Chem. Eng. Data 64 (2019) 4763–4774, doi:10.1021/acs.jced.9b00145.
[3] A. Söldner, J. Zach, B. König, Deep eutectic solvents as extraction media for metal salts and oxides exemplarily shown for phosphates from incinerated sewage sludge ash, Green Chem 21 (2019) 321–328, doi:10.1039/C8GC02702A.
[4] A.P. Abbott, E.I. Ahmed, R.C. Harris, K.S. Ryder, Evaluating water miscible deep eutectic solvents (DESs) and ionic liquids as potential lubricants, Green Chem 16 (2014) 4156, doi:10.1039/C4GC00952E.
[5] A.P. Abbott, G. Frisch, J. Hartley, W.O. Karim, K.S. Ryder, Anodic dissolution of metals in ionic liquids, Prog. Nat. Science: Mater. Int. 25 (2015) 595, doi:10.1016/j.pnsc.2015.11.005.
[6] D. Marino, M. Shalaby, S. Kriescher, M. Wessling Corrosion of metal electrodes in deep eutectic solvents, Electrochem. Commun. 90 (2018) 101, doi:10.1016/j.elecom.2018.04.011.
[7] T. Ibrahim1, R. Alhasan, M. Bedrelzaman, M. Sabri, N. Jabbar, F. Mjalli, Corrosion Behavior of Common Metals in Eutectic Ionic Liquids, Int. J. Electrochem. Sci. 14 (2019) 8450–8469, doi:10.20964/2019.09.27.
[8] A.A. Kityka, Y.D. Rublova, A. Kelm, V.V. Malyshev, N.G. Bannyk, I. Flis-Kabulska, Kinetics and mechanism of corrosion of mild steel in new types of ionic liquids, J, Electroanal. Chem. 823 (2018) 234–244, doi:10.1016/j.jelechem.2018.06.018.
[9] J.R. Davis, Alloying: Understanding the Basics, 351-416, ASM International, 2001.

[10] Edward Ghali, Corrosion Resistance of Aluminum and Magnesium Alloys-Understanding, Performance, and Testing, John Wiley & Sons, Inc., Hoboken, New Jersey, 2010.
[11] F.J. Martin, G.T. Cheek, W.E.O Grady, P.M. Natishan, Impedance studies of the passive film on aluminum, Corr. Sci. 47 (2005) 3187–3201, doi:10.1016/j.corsci.2005.05.058.
[12] K.N. Borba, F. Trombetta, R.F. de Souza, E.M.A. Martini, Stability of Al_2O_3/Al in ionic liquid BMI.BF4/γ-butyrolactone electrolytes for use in electrolytic capacitors, Ionics 23 (2017) 1165–1171, doi:10.1007/s11581-016-1912-x.
[13] P. Neufeld, A.K. Chakrabarty, The corrosion of aluminum and its alloys in anhydrous phenol, Corr. Sci. 12 (1972) 517–525, doi:10.1016/S0010-938X(72)80082-9.
[14] A. Faure-Geors, F. Dalard, A.B. Rais, Characterization of aluminum alloys in tetrahydrofuran media, J. Appl. Electrochem. 19 (1989) 203–206, doi:10.1007/BF01062301.
[15] A.P. Abbott, G. Capper, D.L. Davies, R.K. Rasheed, P. Shikotra, Selective extraction of metals from mixed oxide matrixes using choline-based ionic liquids, Inorg. Chem. 44 (2005) 6497–6499, doi:10.1021/ic0505450.
[16] P. Abbott Andrew, Collins John, Dalrymple Ian, C. Harris Robert, Mistry Reena, Qiu Fulian, Scheirer James, R. Wise William, Processing of electric arc furnace dust using deep eutectic solvents, Aust. J. Chem. 62 (2009) 341–347, doi:10.1071/CH08476.
[17] P. Hronsky, Corrosion behavior of metallic materials in organic media containing hydrogen chloride, Corrosion 37 (1981) 161–170, doi:10.5006/1.3622160.
[18] E. Heitz, et al., Corrosion of metals in organic solvents, page 194, in: M.G. Fontana, et al. (Eds.), Advances in Corrosion Science and Technology, Plenum Press, New York, 1974.
[19] C. Verma, E.E. Ebenso, M.A. Quraishi, Ionic liquids as green and sustainable corrosion inhibitors for metals and alloys: An overview, J. Mol. Liq. 233 (2017) 403–414, doi:10.5772/intechopen.70421.
[20] B. Garcia, M. Armand, Aluminium corrosion in room temperature molten salt, J. Power Sources 132 (2004) 206–208, doi:10.1016/j.jpowsour.2003.12.046.
[21] W. Behl, E. Plichta, Stability of aluminum substrates in lithium-ion battery electrolytes, J. Power Sources 72 (1998) 132–135, doi:10.1016/S0378-7753(97)02700-6.
[22] C. Blanc, G. Mankowski, Susceptibility to pitting corrosion of 6056 aluminium alloy, Corr. Sci. 39 (1997) 949–959, doi:10.1016/S0010-938X(97)81160-2.
[23] W.J. Liang, P.A. Rometsch, L.F. Cao, N. Birbilis, General aspects related to the corrosion of 6xxx series aluminium alloys: Exploring the influence of Mg/Si ratio and Cu, Corr. Sci. 76 (2013) 119–128, doi:10.1016/j.corsci.2013.06.035.
[24] P. Schmutz, G.S. Frankel, Characterization of AA2024-T3 by Scanning Kelvin Probe Force Microscopy, J. Electrochem. Soc. 145 (7) (1998) 2285–2295, doi:10.1149/1.1838633.
[25] W.A. Badawy, S.S. Elegamy, Kh.M. Ismail, Comparative study of tantalum and titanium passive films by electrochemical impedance spectroscopy, Br. Corros. J. 28 (1993) 133–136, doi:10.1179/bcj.1993.28.2.133.
[26] J. Evertsson, F. Bertram, F. Zhang, L. Rullik, L.R. Merte, M. Shipilin, M. Soldemo, S. Ahmadi, N. Vinogradov, F. Carlà, J. Weissenrieder, M. Göthelid, J. Pan, A. Mikkelsen, J.O. Nilsson, E. Lundgren, The thickness of native oxides on aluminum alloys and single crystals, Appl. Surf. Sci. 349 (2015) 826–832, doi:10.1016/j.apsusc.2015.05.043.
[27] L. Peater, J. Arai, Anodic dissolution of aluminum in organic electrolytes containing perfluoroalkylsulfonyl imides, J. Appl. Electrochem. 29 (1999) 1053–1061, doi:10.1023/A:1003573430989.
[28] A. Boag, A.E. Hughes, A.M. Glenn, T.H. Muster, D. McCulloch, Corrosion of AA2024-T3 Part I: Localised corrosion of isolated IM particles, Corros. Sci. 53 (2011) 17–26, doi:10.1016/j.corsci.2010.09.009.
[29] M. Tanaka, T. Warner, T6 and T78 tempers of AA6065 alloy: a quantitative TEM study, Mater. Sci. Forum 331-337 (2000) 983–988, doi:10.4028/www.scientific.net/MSF.331-337.983.
[30] S. Lebouil, A. Duboin, F. Monti, P. Tabeling, V. Volovich, K. Ogle, A novel approach to on-line measurement of gas evolution kinetics: Application to the negative difference effect of Mg in chloride solution, Electrochim. Acta 124 (2014) 176–182, doi:10.1016/j.electacta.2013.07.131.
[31] E. Mc Cafferty, Sequence of steps in the pitting of aluminum by chloride ions, Corros. Sci. 45 (2003) 1421–1438, doi:10.1016/S0010-938X(02)00231-7.
[32] M Liu, Y. Jin, C. Zhang, C. Leygraf, L. Wen, Density-functional theory investigation of Al pitting corrosion in electrolyte containing chloride ions, Appl. Surf. Sci. 357 (2015) 2028–2038, doi:10.1016/j.apsusc.2015.09.180.
[33] R. Costa, M. Figueiredo, C.M. Pereira, F. Silva, Electrochemical double layer at the interfaces of Hg/choline chloride based solvents, Electrochim. Acta 55 (2010) 8916–8920, doi:10.1016/j.electacta.2010.07.070.
[34] O.S. Hammond, H. LI, C. Westermann, F. Endres, A.Y.M. Al-Murshedi, A.P. Abbott, G. Warr, K.J. Edler, R. Atkin, Nanostructure of the deep eutectic solvent/platinum electrode interface as a function of potential and water content, Nanoscale Horiz 4 (2019) 158–168, doi:10.1039/C8NH00272J.
[35] A.P. Abbott, F. Qiu, H.M.A. Abood, M.R. Ali, K.S. Ryder, Double layer, diluent and anode effects upon the electrodeposition of aluminium from chloroaluminate based ionic liquids, Phys. Chem. Chem. Phys. 12 (2010) 1862–1872, doi:10.1039/B917351J.
[36] B.A. Abd-El-Nabey, N. Khalil, M.M. Eisa, Pitting corrosion of stainless steel in water-organic solvent mixtures: II, Surf. Technol. 22 (1984) 9–14, doi:10.1016/0376-4583(84)90023-2.
[37] J.W. Tester, H.S. Isaacs, Diffusional effects in simulated localized corrosion, J. Electrochem. Soc. 122 (1975) 1435–1438, doi:10.1149/1.2134039.